Supplementary videos

Supplementary Video 1: Visualization of blood flow *in vivo.* Top panel: original photoacoustic images. Bottom panel: masked images after spatiotemporal filtering.
Supplementary Video 2: Phantom validation. Top panel: subbranch C_1. Middle panel: subbranch C_2. Bottom panel: main branch C_3.
Supplementary Video 3: *In vivo* blood flow of a vessel with a varying diameter. Top panel: original photoacoustic images. Bottom panel: masked images after spatiotemporal filtering.
Supplementary Video 4: *In vivo* blood flow of a vessel at an isosbestic wavelength. Top panel: original photoacoustic images. Bottom panel: masked images after spatiotemporal filtering.
Supplementary Video 5: *In vivo* blood flow at different wavelengths. Top panel: photoacoustic images acquired at an optical wavelength of 750 nm. Middle panel: photoacoustic images acquired at an optical wavelength of 805 nm. Bottom panel: photoacoustic images acquired at an optical wavelength of 900 nm.
Supplementary Video 6: *In vivo* blood flow of a vessel at a depth of 3.5 mm. Top panel: original photoacoustic images. Bottom panel: masked images after spatiotemporal filtering.
Supplementary Video 7: *In vivo* blood flow of a vessel at a depth of 5.5 mm. Top panel: original photoacoustic images. Bottom panel: masked images after spatiotemporal filtering.
Supplementary Video 8: *In vivo* haemodynamics around a valve. Top panel: original photoacoustic images. Bottom panel: masked images after spatiotemporal filtering.
Supplementary Video 9: Measuring functional responses to a blood pressure cuff. Top panel: time lapse of fractional speed and velocity vectors overlaid on the vessel structure. Bottom panel: time lapse of the fractional speed change.
Supplementary Video 10: Measuring blood flow in artery #1. Top panel: original photoacoustic images. Bottom panel: masked images after spatiotemporal filtering.
Supplementary Video 11: Measuring blood flow in artery #2. Top panel: original photoacoustic images. Bottom panel: masked images after spatiotemporal filtering.
Supplementary Video 12: Imaging time-variant blood flow.

Supplementary figures

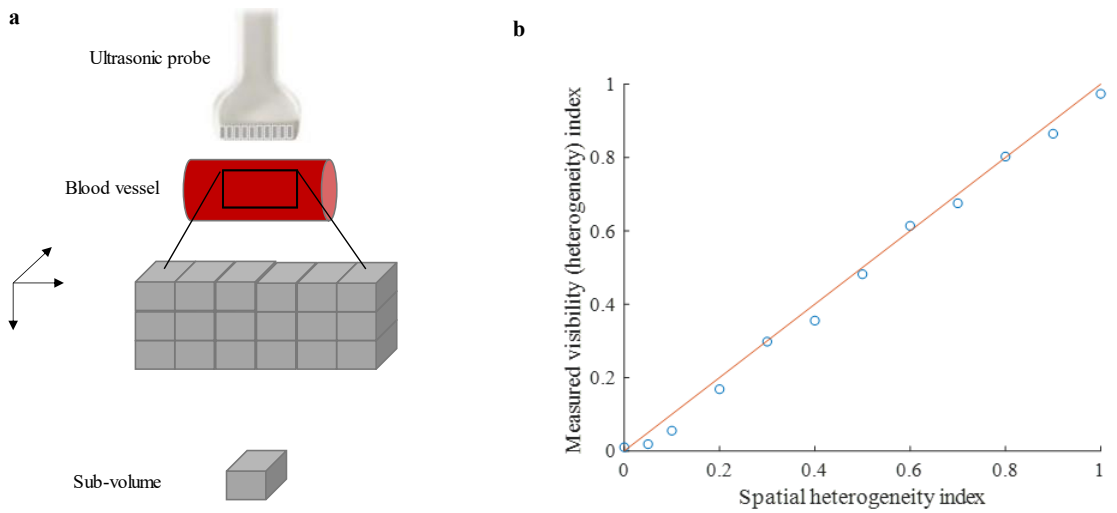

Supplementary Fig. 1 | Model the spatial heterogeneity of the blood. a, Model and simulation setup for the spatial heterogeneity analysis of the blood and its effect on photoacoustic signals. **b,** Relationship between the measured relative visibility (heterogeneity) index and the defined spatial heterogeneity.

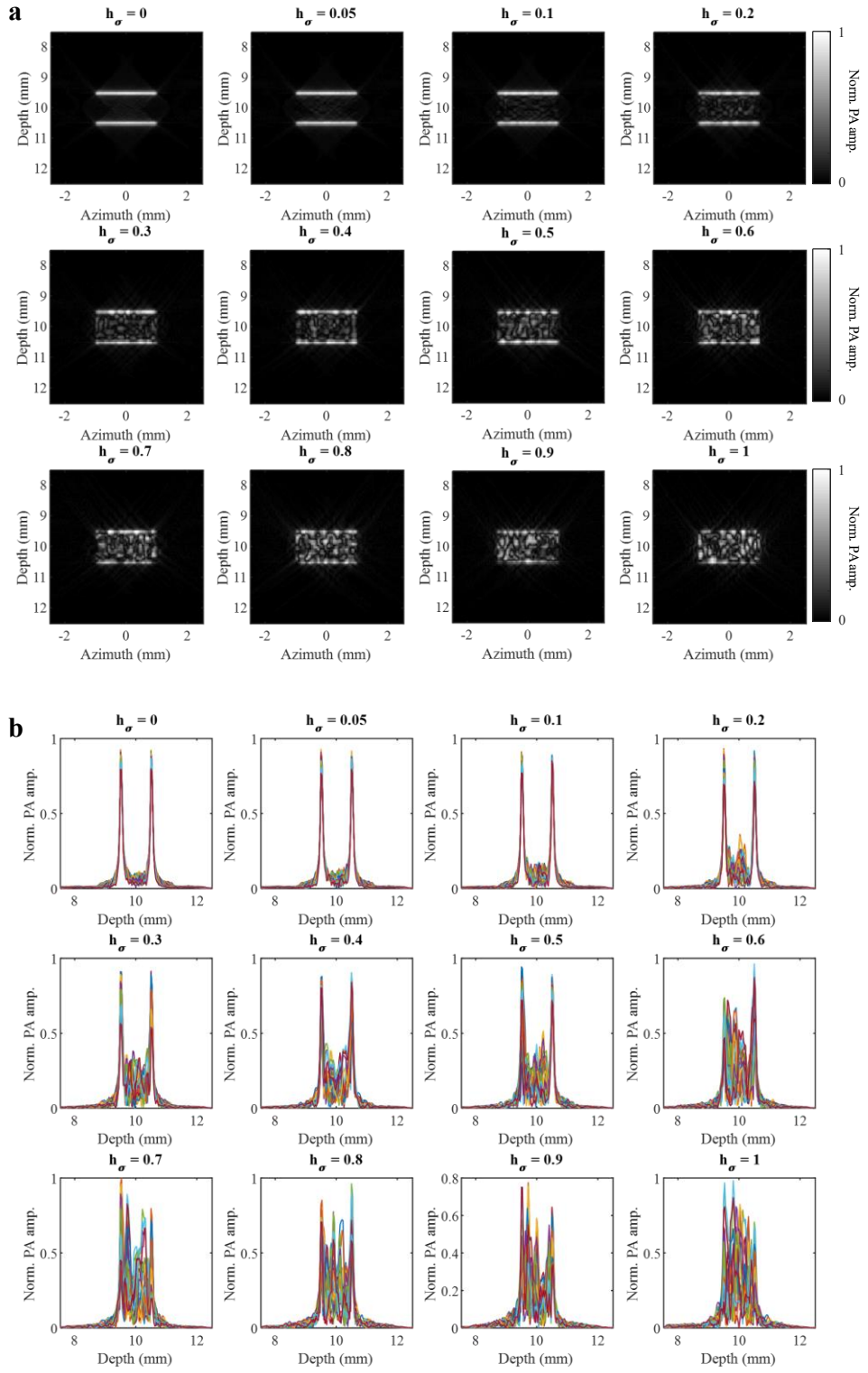

Supplementary Fig. 2 | Simulation of spatial heterogeneity. a, Photoacoustic images with the spatial heterogeneity index varied from 0 to 1. **b,** Profiles of photoacoustic images with the spatial heterogeneity index varied from 0 to 1.

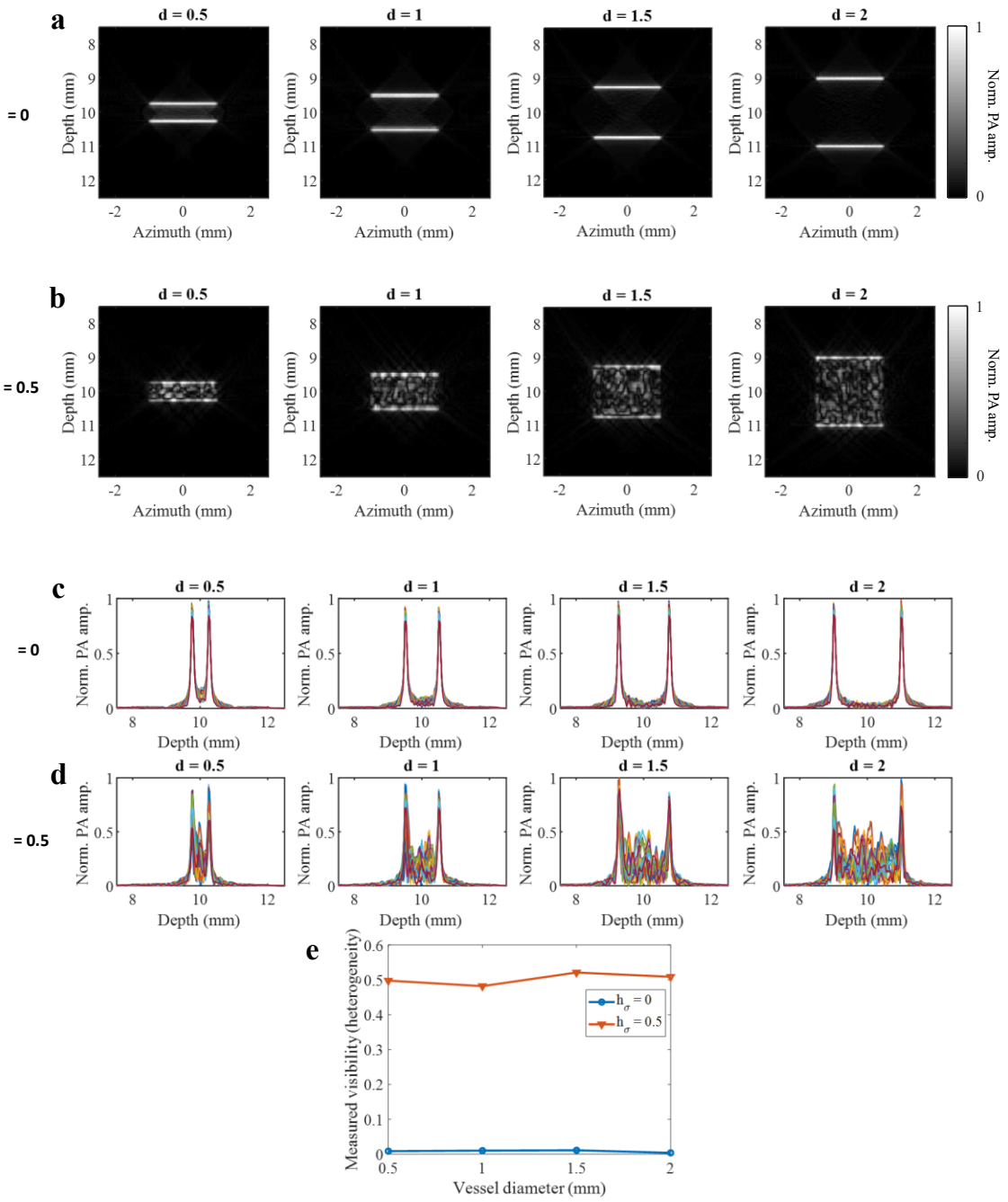

Supplementary Fig. 3 | Analysis of spatial heterogeneity. a, Photoacoustic images with the vessel diameter varied among 0.5 mm, 1.0 mm, 1.5 mm and 2.0 mm at spatial heterogeneity index 0. **b,** Photoacoustic images with the vessel diameter varied among 0.5 mm, 1.0 mm, 1.5 mm and 2.0 mm at spatial heterogeneity index 0.5. **c,** Profiles of photoacoustic images with the vessel diameter varied among 0.5 mm, 1.0 mm, 1. 5 mm and 2.0 mm at spatial heterogeneity index 0. **d,** Profiles of photoacoustic images with the vessel diameter varied among 0.5 mm, 1.0 mm, 1.5 mm and 2.0 mm at spatial heterogeneity index 0.5. **e,** Relationship between the measured visibility (heterogeneity) and the vessel diameter.

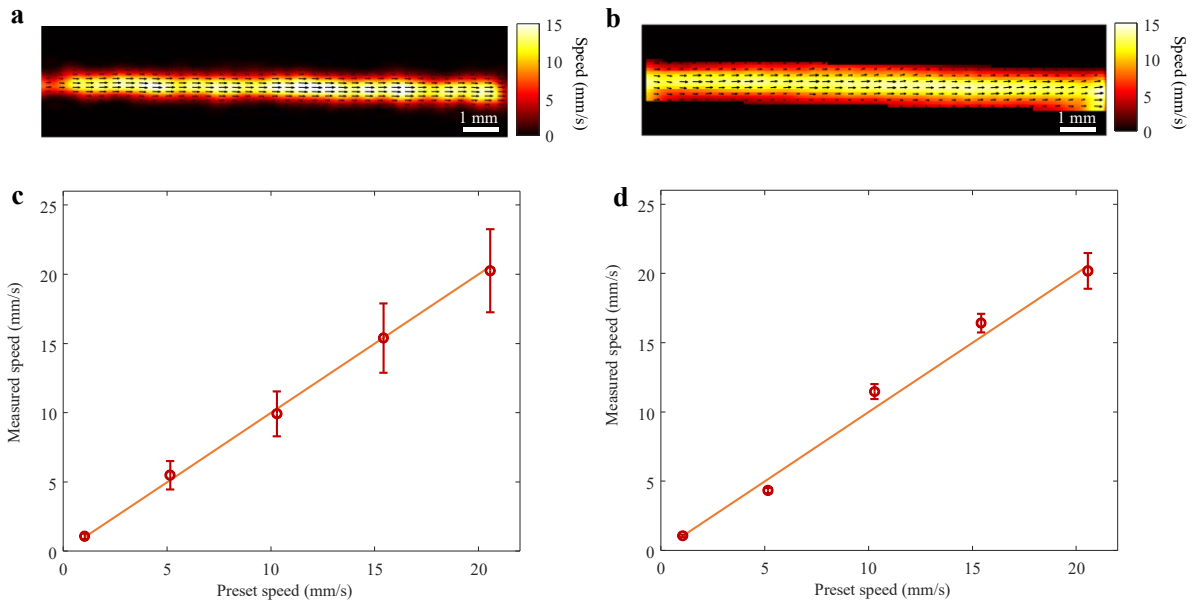

Supplementary Fig. 4 | Phantom flow validation with ultrasound. a-b, Representative photoacoustic and ultrasound vector flow maps for the phantom with a mean flow speed of 10.28 mm/s as a ground truth. **c,** Measured flow speeds plotted against preset syringe flow speeds. The mean ± standard deviation (in mm/s) speeds were (from left to right): 1.07 ± 0.21, 5.33 ± 0.85, 9.93 ± 1.83, 14.77 ± 2.76, and 20.14 ± 3.17 with relative errors of 4.5, 3.6, 3.4, 4.2, and 2.0%, respectively. **d**, Measured ultrasound flow speeds plotted against preset syringe flow speeds. The mean ± standard deviation (in mm/s) speeds were (from left to right): 1.06 ± 0.08, 4.39 ± 0.19, 11.16 ± 0.57, 16.43 ± 0.67, and 20.20 ± 1.28 with relative errors of 3.4, 14.5, 8.6, 6.6, and 1.8 %, respectively. Orange line represents the preset speed, and red circles represent the measured mean speeds. Error bars represent the standard deviation for each measurement.

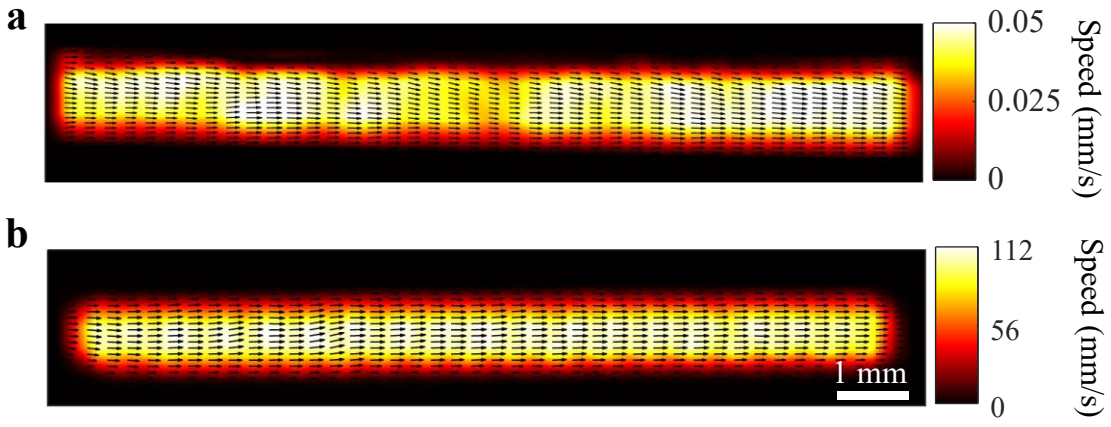

Supplementary Fig. 5 | Upper and lower limits of speed detection. a, Vector flow map of a phantom with a mean flow speed of 0.04 mm/s as a ground truth. **b,** Vector flow map of a phantom with a mean flow speed of 102.79 mm/s as a ground truth. The measured mean speeds (in mm/s) for **a**–**b** were 0.039 mm/s (n = 19364) and 96.30 (n = 13300) with relative errors of 4.3 and 7.9%, respectively.

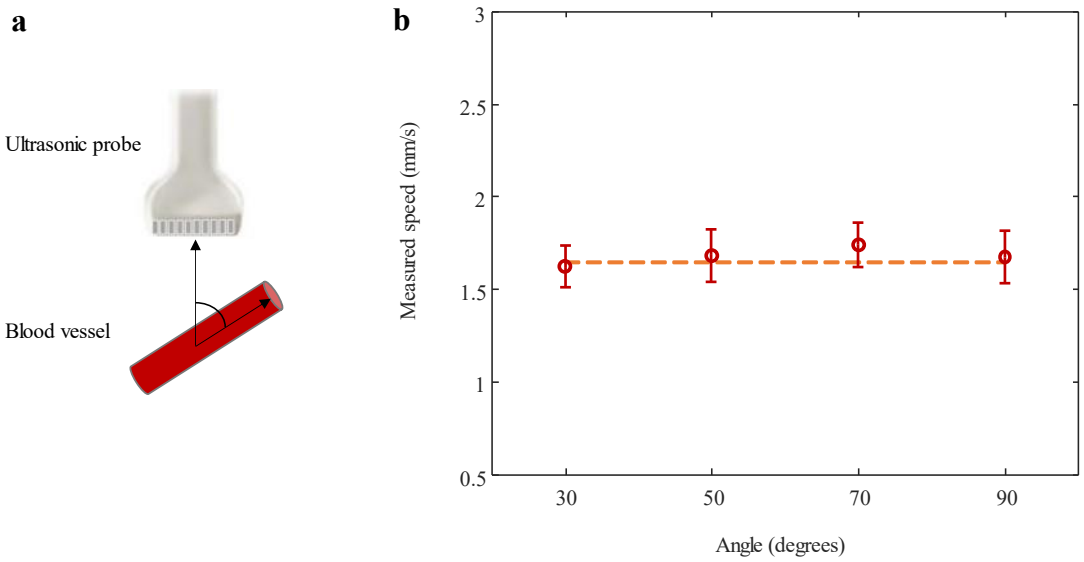

Supplementary Fig. 6 | Flow measurement with varied angles. a, Schematic of the probe axis and the blood vessel with an angle θ. **b,** The relationship between the measured speed and the angle θ by PAVT. The mean $\pm$ standard deviation (in mm/s) speeds were (from left to right) 1.62 $\pm$ 0.11, 1.68 $\pm$ 0.14, 1.74 $\pm$ 0.12, and 1.67 $\pm$ 0.14, respectively. Error bars represent the standard deviation for each measurement. Orange dashed line represents the ground truth of 1.64 mm/s.

663

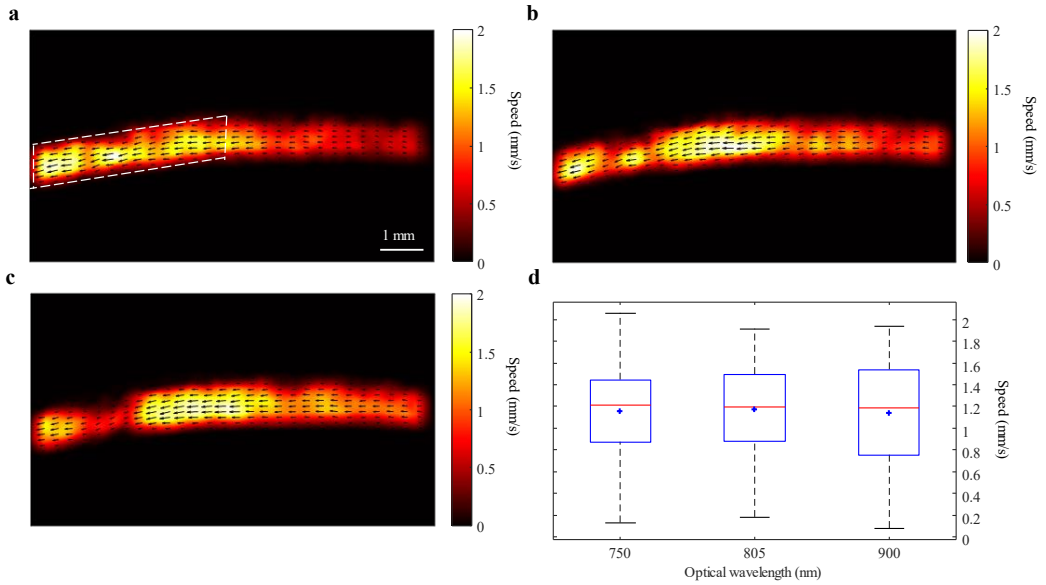

Supplementary Fig. 7 | PAVT at multiple wavelengths. A blood vessel in the palmar region was imaged at three different optical wavelengths in the near-infrared spectral region. **a–c**, Vector flow maps for the vessel imaged at 750, 805, and 900 nm, respectively. **d,** Box-and-whisker plot of measured speeds at each wavelength. The mean speeds (in mm/s) for wavelengths of 705, 805, and 900 nm were 1.1, 1.17, and 1.14, respectively (n = 9971). The red horizontal line shows the median; the boxes indicate the 25th and 75th percentiles; the blue cross shows the mean value. The White box indicates the region for speed calculations.

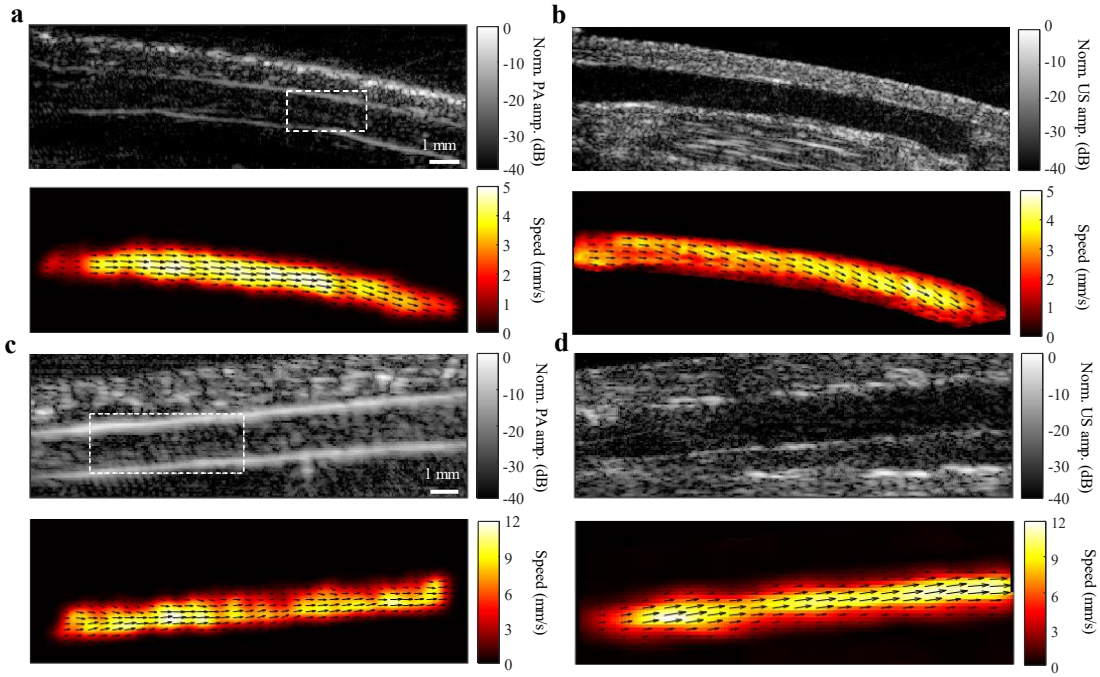

Supplementary Fig. 8 | *In vivo* flow validation with ultrasound. a–b, Photoacoustic and ultrasound structural images (top) and vector flow maps (bottom) of a vessel with slow blood flow in the forearm. The mean ± standard deviation (in mm/s) speeds across the region indicated by the white box for PAVT and ultrasound were 3.55 ± 0.10 and 3.38 ± 0.14 (n = 588), respectively). **c–d**, Photoacoustic and ultrasound structural images (top) and vector flow maps (bottom) of a vessel with fast blood flow in the forearm. The mean ± standard deviation (in mm/s) speeds across the region indicated by the white box for PAVT and ultrasound were 8.50 ± 1.14 and 8.14 ± 1.00 (n = 3094), respectively. Discrepancies in the speed maps can be due to non-simultaneous measurements.

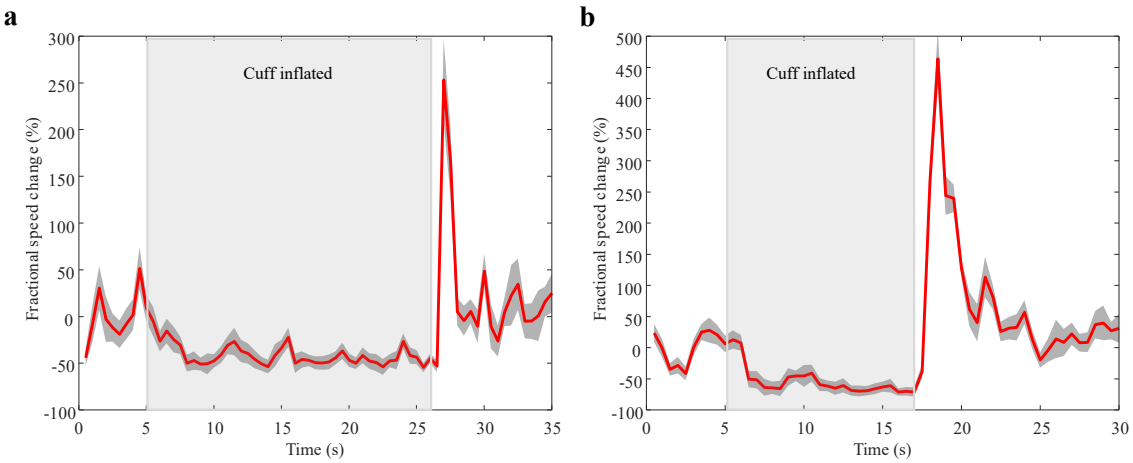

Supplementary Fig. 9 | Flow response to blood pressure cuff. Fractional flow speed responses to a blood pressure cuff were measured for different subjects in different regions. For each trial the cuff was applied to the brachial vein. **a**, Fractional flow speed response in a metacarpal vein. **b**, Fractional flow speed response in a carpal tunnel vein.

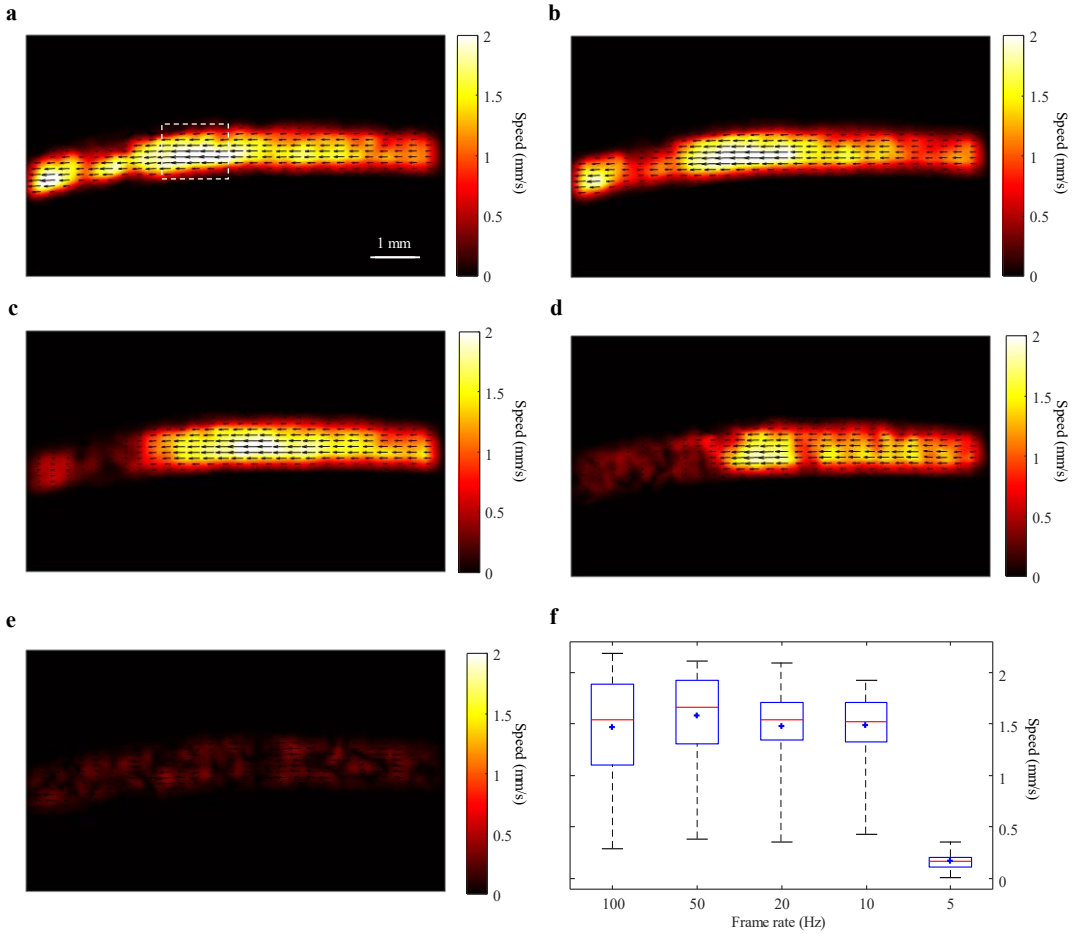

Supplementary Fig. 10 | Effect of downsampling. Images of a palmar vessel were acquired for one second at a pulse repetition frequency (PRF) of 100 Hz. **a–e,** Vector flow maps for sampling the images at frame rates of 100, 50, 20, 10, and 5 Hz, respectively. **f,** Box-and-whisker plot of measured speeds at each frame rate. The mean speeds (in mm/s) for frame rates of 100, 50, 20, 10, and 5 Hz were 1.47, 1.58, 1.48, 1.49, and 0.16, respectively (n = 2952). The red horizontal line shows the median; the boxes indicate the 25th and 75th percentiles; the blue cross shows the mean value. White box indicates the region for speed calculations.

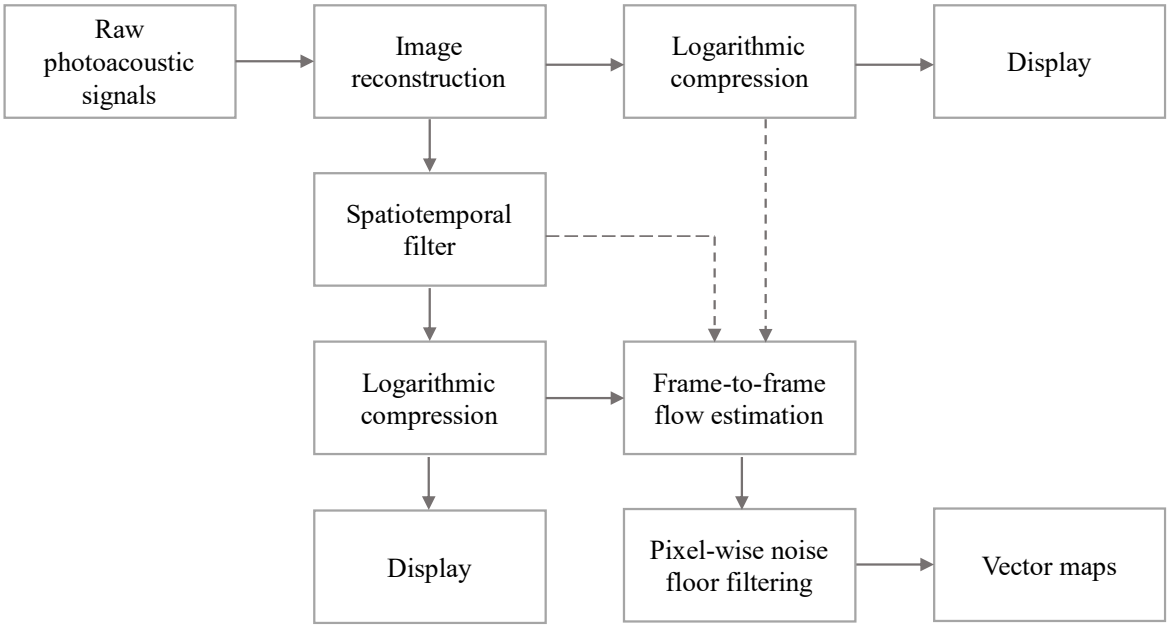

Supplementary Fig. 11 | Data processing flowchart. We first applied an image reconstruction algorithm to the raw photoacoustic signals to obtain the reconstructed images. We then performed logarithmic compression on the reconstructed images for obtaining the structure images of the blood vessel and to directly visualize the blood flow. Alternatively, for clearer blood flow visualization, we applied a singular value decomposition (SVD)-based spatiotemporal filter to the reconstructed images and then performed logarithmic compression on the filtered images. Lastly, we used a frame-to-frame flow estimation algorithm and pixel-wise noise floor filtering to obtain the vector maps of the blood flow.

672

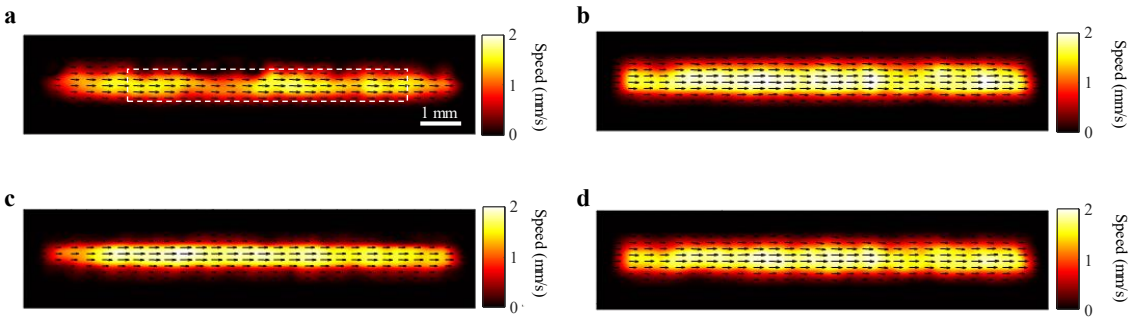

Supplementary Fig. 12 | Effect of SVD and logarithmic compression. Images of a blood phantom with a mean flow speed of 1.645 mm/s were acquired as a ground truth. **a–b,** Vector flow maps obtained from processing the images on a linear scale with and without SVD processing, respectively. **c–d** Vector flow maps obtained from processing the images on a logarithmic scale with and without SVD processing, respectively. The mean speeds (in mm/s) across the region indicated by the white box for **a–d** were 1.154, 1.758, 1.622, and 1.640 with relative errors 29, 6.9, 1.4, and 0.3 % respectively (n = 5599).

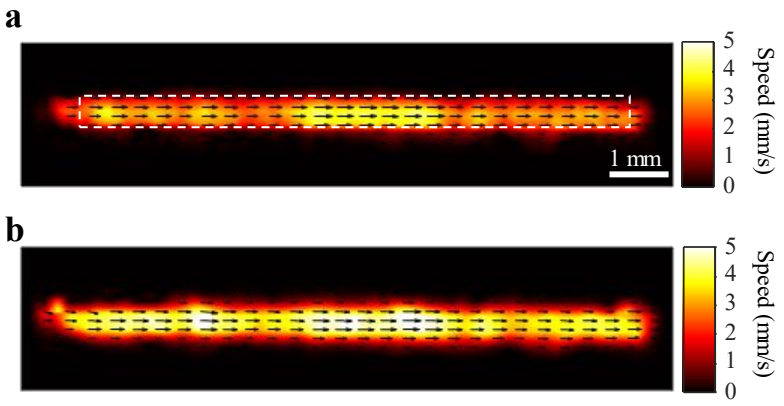

Supplementary Fig. 13 | Effect of noise floor filtering. Images of a blood phantom with a mean flow speed of 4.11 mm/s were acquired as a ground truth. **a,** Vector flow map obtained from averaging across all frames for each pixel. **b,** Vector flow map obtained from averaging after performing noise floor filtering for each pixel. The mean speeds (in mm/s) across the region indicated by the white box for **a**–**b** were 3.93 (n = 6232) and 4.12 (n = 6232) with relative errors of 4.5 and 0.9 %, respectively.

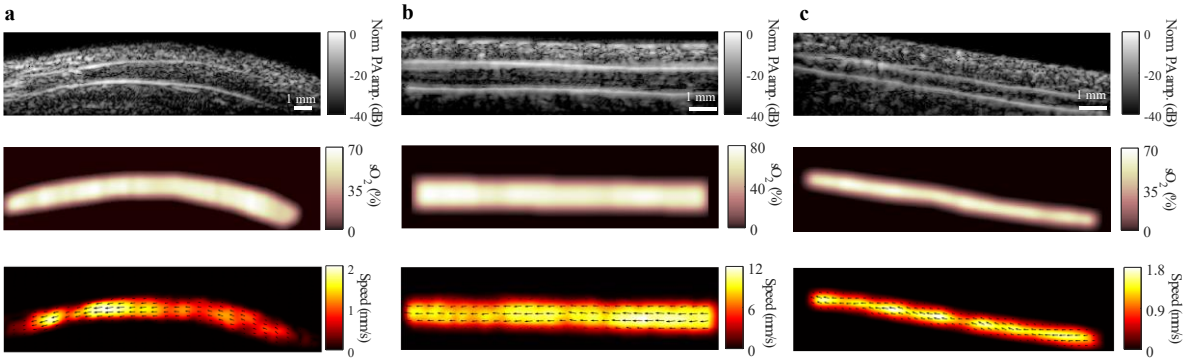

Supplementary Fig. 14 | Simultaneous measurement of hemoglobin oxygen saturation (sO_2) and blood flow. a–c, Photoacoustic structure image (top panel), sO_2 map (middle panel), and vector flow map (bottom panel) of three vessels located in the palmar region, carpal tunnel region and forearm region, respectively.

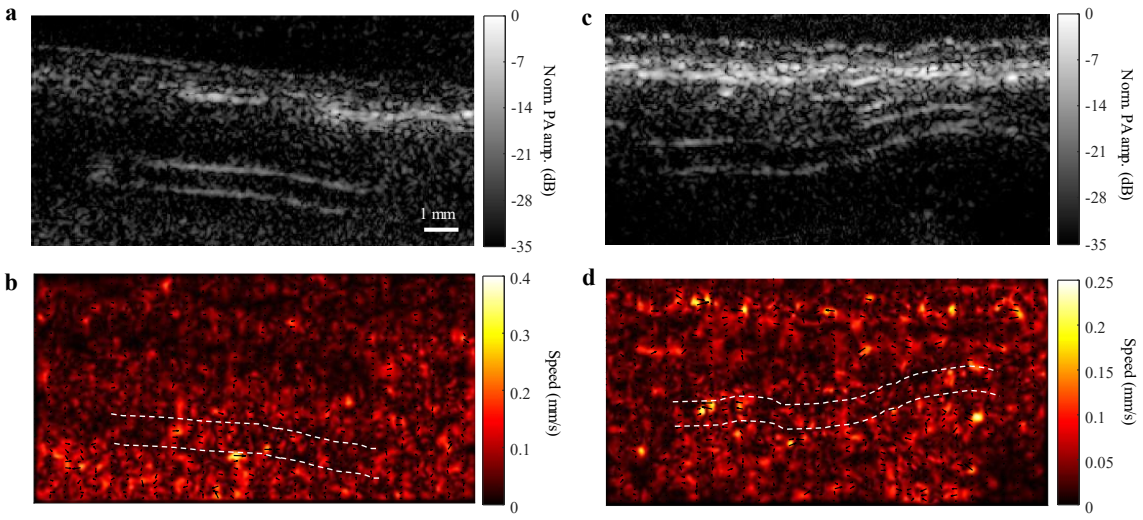

Supplementary Fig. 15 | Measuring blood flow in arteries. Two blood vessels in the hand region were imaged. **a–b**, Structure and vector flow maps for an artery at a depth of 3 mm. **c–d**, structure and vector flow maps for another artery at a depth of 2.5 – 3 mm. White dashed lines indicate the vessel region.